

# Probing the gamma-ray variability in 3C 279 using broadband observations

B. Rani<sup>1,2\*</sup>, T. P. Krichbaum<sup>2</sup>, S.-S. Lee<sup>3,4</sup>, K. Sokolovsky<sup>5,6,7</sup>, S. Kang<sup>3,4</sup>,  
D.-Y. Byun<sup>3,4</sup>, D. Mosunova<sup>5</sup>, J. A. Zensus<sup>2</sup>

<sup>1</sup>NASA Goddard Space Flight Center, Greenbelt, MD 20771, USA

<sup>2</sup>Max-Planck-Institut für Radioastronomie (MPIfR), Auf dem Hügel 69, D-53121 Bonn, Germany

<sup>3</sup>Korea Astronomy and Space Science Institute, 776 Daedeok-daero, Yuseong-gu, Daejeon 34055, Korea

<sup>4</sup>University of Science and Technology, 217 Gajeong-ro, Yuseong-gu, Daejeon 34055, Korea

<sup>5</sup>Astro Space Center of Lebedev Physical Institute, Profsoyuznaya 84/32, 117997 Moscow, Russia

<sup>6</sup>IAASARS, National Observatory of Athens, Vas. Pavlou & I. Metaxa, GR-15 236 Penteli, Greece

<sup>7</sup>Sternberg Astronomical Institute, Moscow State University, Universitetskii pr. 13, 119992 Moscow, Russia

Accepted — . Received —

## ABSTRACT

We present the results of a broadband radio-to-GeV observing campaign organized to get a better understanding of the radiation processes responsible for the  $\gamma$ -ray flares observed in 3C 279. The total intensity and polarization observations of the source were carried out between December 28, 2013 and January 03, 2014 using the *Fermi*-LAT, *Swift*-XRT, *Swift*-UVOT, and KVN telescopes. A prominent flare observed in the optical/near-UV passbands was found to be correlated with a concurrent  $\gamma$ -ray flare at a confidence level  $>95\%$ , which suggests a co-spatial origin of the two. Moreover, the flaring activity in the two regimes was accompanied by no significant spectral variations. A peak in the X-ray light curve coincides with the peaks of the fractional polarization curves at 43 and 86 GHz radio bands. No prominent variation was noticed for the total intensity and the electric vector position angle (EVPA) observations at radio bands during this period. We noticed a possible hint of steepening of the radio spectrum with an increase in percentage polarization, which suggests that the radio polarization variations could be simply due to a spectral change. In a simple scenario, the correlated optical/ $\gamma$ -ray flares could be caused by the same population of emitting particles. The coincidence of the increase in radio polarization with the X-ray flux supports the picture that X-rays are produced via inverse-Compton scattering of radio photons. The observed fractional variability for the  $\gamma$ -ray flare  $\sim 0.23$  does not exceed that in the optical regime, which is inconsistent with what we usually observe for 3C 279; it could be due to different dependencies of the magnetic field and the external radiation field energy density profiles along the jet.

**Key words:** galaxies: active – quasars: individual: 3C 279 – radio continuum: galaxies – jets: galaxies – gamma-rays – galaxies: X-rays

## 1 INTRODUCTION

Powered by accretion onto super-massive black holes (with masses up to  $\sim 10^{10} M_{\odot}$ ), active galactic nuclei are extremely bright objects in the extra-galactic sky. In a small sub-group of these objects, a substantial fraction of accretion energy is converted into kinetic energy forming highly collimated and relativistic outflows of energetic plasma and magnetic fields, called jets. Blazars with their jets pointing close to our line-of-sight are strong emitters of electromagnetic radiation over a range of more than 20 decades

in energy. Because of relativistic beaming, these sources can be detected out to much larger distances than unbeamed objects. BL Lacertae objects (BL Lacs) and flat spectrum radio quasars (FSRQs) are clubbed together and called blazars, in spite of the dissimilarity of their optical spectra – FSRQs show strong broad emission lines, while BL Lacs have only weak or no emission lines in their optical spectra. Blazars are notable for showing variability on a range of timescales that is often described as a superposition of multiple flares. Despite several efforts to understand the broadband flaring activity of blazars, the exact origin of variability is still debated. Of particular interest is the question why for the same source sometimes we do see correlated behavior in different energy bands and sometimes we do not.

\* NPP Fellow

The flat spectrum radio quasar (FSRQ) 3C 279 (at  $z = 0.538$  [Burbidge & Rosenberg 1965](#)) is one of the most intensively studied objects of its class. The source has an estimated black hole mass in the range of  $(3\text{--}8)\times 10^8 M_\odot$  derived independently from the luminosity of broad optical emission lines ([Woo & Urry 2002](#)) and from the width of the  $H_\beta$  line ([Gu et al. 2001](#)). Owing to its high flux density and prominent variations in total intensity and polarization, 3C 279 is an excellent candidate to examine physics of extragalactic jets and to understand particle acceleration to high energies. It has been monitored intensively at radio, optical, and more recently also X-ray and  $\gamma$ -ray frequencies and has been the subject of intensive multi-wavelength campaigns (e.g., [Maraschi et al. 1994](#); [Hartman et al. 1996](#); [Chatterjee et al. 2008](#); [Wehrle et al. 1998](#); [Larionov et al. 2008](#); [Collmar et al. 2010](#); [Böttcher et al. 2007](#); [Hayashida et al. 2012, 2015](#); [Kang et al. 2015](#)). In 2006, emission at very high energies ( $E > 100$  GeV) was detected from 3C 279 with the Major Atmospheric Gamma-Ray Imaging Cherenkov (MAGIC) telescope ([Albert et al. 2008](#)).

The source has a bright radio jet extending up to kiloparsec scales. The very long baseline interferometry (VLBI) observations have measured apparent velocities from 4 to 20  $c$  in the parsec scale region of the jet, which is aligned close to the observer's line-of-sight ( $\lesssim 2^\circ$ , [Lister et al. 2013](#); [Jorstad et al. 2004](#)). Polarimetric observations have detected both linearly and circularly polarized emission from the parsec-scale jet of 3C 279 ([Wardle et al. 1998](#); [Taylor 2000](#); [Homan et al. 2009](#)). Additionally, the observed optical radiation is also highly polarized (linear polarization up to 45.5% in the U band [Mead et al. 1990](#)). [Wagner & Mannheim \(2001\)](#) detected variable optical circular polarization in 3C 279 exceeding 1%. [Abdo et al. \(2010a\)](#) reported a coincidence of an optical polarization angle swing with a bright  $\gamma$ -ray flare in the source, which suggests a highly ordered configuration of magnetic field during the emission of bright  $\gamma$ -ray flares.

The source has been detected by the LAT (Large Area Telescope) on board the *Fermi Gamma-ray Space Telescope* since its launch in 2008 ([Abdo et al. 2010b](#)). Being one of the brightest and most rapidly variable sources in the GeV regime, 3C 279 has been the subject of several recent multi-wavelength campaigns ([Hayashida et al. 2012, 2015](#)). Multiple  $\gamma$ -ray outbursts have been detected in the source ([Hayashida et al. 2015](#); [Paliya 2015](#)). In December 2013, a series of  $\gamma$ -ray flares were observed, reaching the highest flux level measured in this object since the beginning of the *Fermi* mission, with  $F(E > 100 \text{ MeV})$  of  $10^{-5} \text{ photons cm}^{-2} \text{ s}^{-1}$  and a flux-doubling time scale as short as 2 hr ([Hayashida et al. 2015](#)). In June 2015, 3C 279 was observed in an exceptionally bright state ([Cutini 2015](#)) with the highest measured flux,  $F(E > 100 \text{ MeV})$  of  $3.9 \times 10^{-5} \text{ photons cm}^{-2} \text{ s}^{-1}$  ([Paliya 2015](#)), breaking its own record.

Extremely bright flashes of light in the high-energy (GeV/TeV) regime at minutes to hours timescales in blazars have attracted the attention of astronomers, as this suggests that particles can be promptly accelerated with very high efficiency in tiny magnetized emission regions. The rapid variations in the high-energy regime are not always accompanied by flaring activity at other frequencies ([Rani et al. 2013a, 2015](#); [Abdo et al. 2010a](#); [Hayashida et al. 2012](#)), making it even more difficult to understand the radiation processes and acceleration mechanisms involved.

In the following, we present the results of our study of 3C 279 from a multi-wavelength campaign organized in December 2013, when it went through a series of rapid  $\gamma$ -ray flares. We monitored the source using both ground- and space-based telescopes for a time period between December 28, 2013 and January 03, 2014. The aim of our study is to understand the origin of the observed flaring ac-

tivity. More specifically, we investigate the correlation of the  $\gamma$ -ray activity with the emission at lower frequencies.

The paper is structured as follows. Section 2 provides a brief description of observations and data reduction. In Section 3, we report our results. Finally, discussion and conclusions are given in Section 4.

## 2 MULTIFREQUENCY DATA: OBSERVATIONS AND DATA REDUCTION

From December 28, 2013, to January 03, 2014, the broadband flaring activity of the FSRQ 3C 279 was extensively covered using both ground- and space-based observing facilities. The following sub-sections summarize the observations and data reduction.

### 2.1 Radio observations

Single-dish flux density and polarization observations of the source were performed using the radio telescopes at individual KVN (Korean VLBI Network<sup>1</sup> [Lee et al. 2011, 2014](#)) observatories. Observations at 22 GHz were carried out quasi-simultaneously using KVN Tamna, at 43 GHz using KVN Tamna and KVN Yonsei, and at 86 GHz using KVN Yonsei. Polarimetric observations of the source were performed via on-off switching observations with the on-source integration time of  $\sim 6$  minutes. Cross-scan pointing and antenna gain calibration measurements were conducted before every polarimetric observation. We obtained wide-band (512 MHz band-width) spectral measurements with the real and imaginary parts of their cross-correlation for the polarimetric observations. The channel spacing was 125 kHz for 4096 spectral channels. The degree of linear polarization and the electric vector position angle (EVPA) of the source were estimated using a data reduction pipeline presented in [Kang et al. \(2015\)](#), and the rms uncertainties of the linear polarization observations were about 10 mJy and 15 mJy at 22 GHz and 43 GHz, respectively. The statistical uncertainties of the polarization angle measurements were  $\lesssim 0.2^\circ$  and  $\lesssim 0.3^\circ$  at 22 GHz and 43 GHz, respectively. The systematic error of the polarization angle measurements is  $2^\circ$  at both frequencies. The rms uncertainty of the linear polarization observation is about 30 mJy at 86 GHz, and the statistical uncertainty of the polarization angle measurements is  $< 0.5^\circ$  at 86 GHz. The systematic error of  $2^\circ$  of the polarization angle measurements is also applicable to the 86 GHz data. Details about the data reduction pipeline for the polarimetric observations and the polarimetric capability of the KVN are given by [Kang et al. \(2015\)](#). The observed radio flux and polarization curves are shown in Fig. 1 (f to h).

### 2.2 Optical/UV observations

*Swift*-UVOT ([Romney et al. 2005](#)) observed 3C 279 in optical V and near-ultraviolet M2 filters during our campaign period. Multi-extension FITS files containing all images of the target obtained on a specific date were split into single-exposure image files to preserve time resolution. All images were visually inspected to discard the few affected by tracking errors. We used the *uvotsources* tool from HEASoft v6.16 to extract the source counts from a  $5''$ -radius aperture and convert them to magnitudes on the Vega scale ([Poole et al. 2008](#)). The background was estimated in an aperture

<sup>1</sup> <http://kvn.kasi.re.kr>

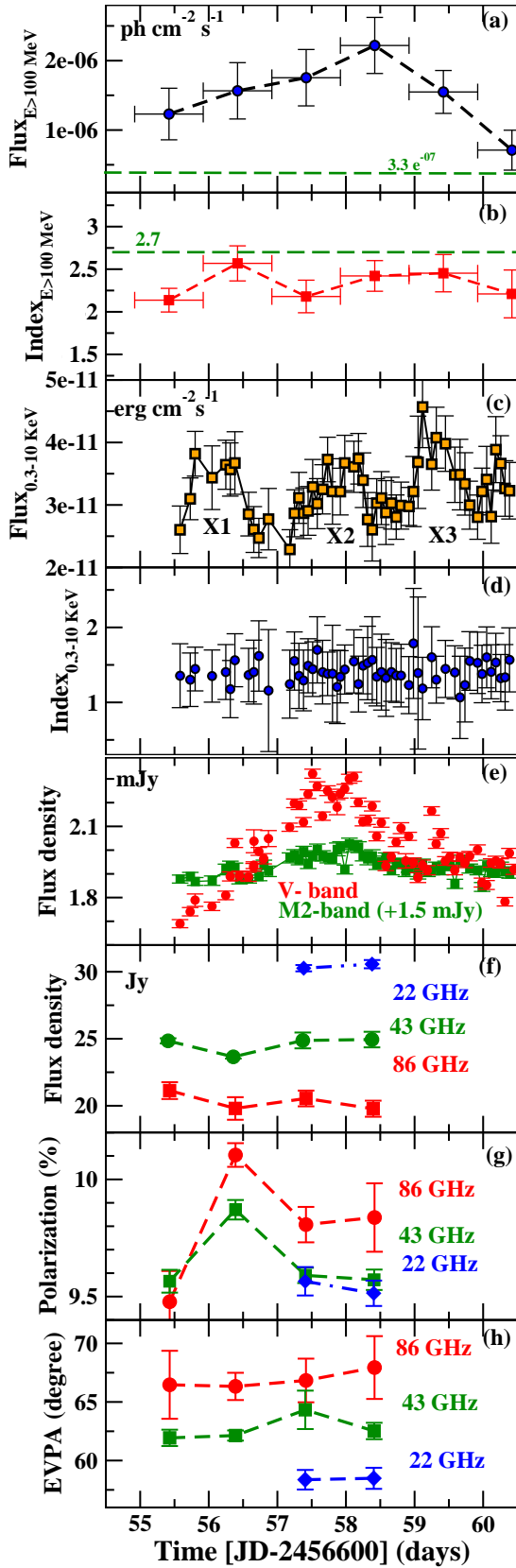


**Figure 1.** Multi-wavelength observations of 3C 279:  $\gamma$ -ray photon flux (a) and photon index (b) light curves for  $E > 100$  MeV (the dashed green line marks the quiescent photon flux and index level); X-ray flux (c) and index (d) light curves for 0.3–10 KeV; optical V and near-UV M2 passband (with a 1.5 mJy offset) flux density light curves (e); radio flux density (f), polarization (g), and EVPA (h) light curves at 22, 43, and 86 GHz bands.

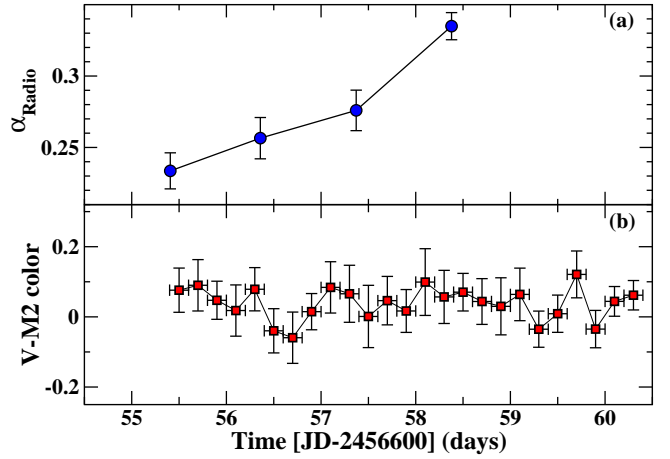


**Figure 2.** Top: Radio spectral index variations. Bottom: Optical V-M2 color index variations.

annulus centered on the source, with an inner radius of  $10''$  and outer radius of  $23''$  chosen to include just the background, avoiding nearby objects.

As a consistency check, we repeated the aperture photometry measurements in V band using the VaST code<sup>2</sup> that relies on SExtractor<sup>3</sup> (Bertin & Arnouts 1996) for source detection and photometry. The magnitude scale was set with comparison stars suggested for ground-based observations<sup>4</sup>. While the individual measurements obtained with the two methods agree within the errors, on average the measurements obtained using the second method are 3.5% brighter. This difference is dominated by uncertainty in reconstructing the non-linear detector response using the small number of comparison stars in the field. The magnitude to flux conversion was done using the central wavelengths for each filter as calibrated by Poole et al. (2008). The observed optical and near-UV light curves extracted using the UVOTSOURCE tool are presented in Fig. 1 (e).

### 2.3 X-ray observations

We analyzed 54 *Swift*-XRT (Burrows et al. 2005) observations of 3C 279 obtained in the photon counting mode simultaneously with *Swift*-UVOT. After pre-processing with XRTPIPELINE v0.13.2, the spectra were extracted from a 20 pixel-radius aperture centered on the object position, grouped to contain at least 25 counts in each energy bin and modeled with XSPEC v12.9.0. The absorbed power law with the total HI column density fixed to the Galactic value ( $N_{\text{HI}} = 0.212 \times 10^{21}$ , Kalberla et al. 2005) provides an acceptable ( $p = 0.01$ ) fit to the 0.3–10 keV spectrum at all epochs. The X-ray photon index shows no significant changes over the course of our observations Fig. 1 (d). The X-ray flux (Fig. 1 c) is therefore extracted keeping the photon index value fixed to 1.46.

### 2.4 Gamma-ray observations

At GeV energies, the source was observed in survey mode by the *Fermi*-LAT (Atwood et al. 2009). We employed here the 100 MeV

<sup>2</sup> <http://scan.sai.msu.ru/vast/>

<sup>3</sup> <http://www.astromatic.net/software/sextractor>

<sup>4</sup> <http://www.lsw.uni-heidelberg.de/projects/extragalactic/charts/1253-055>

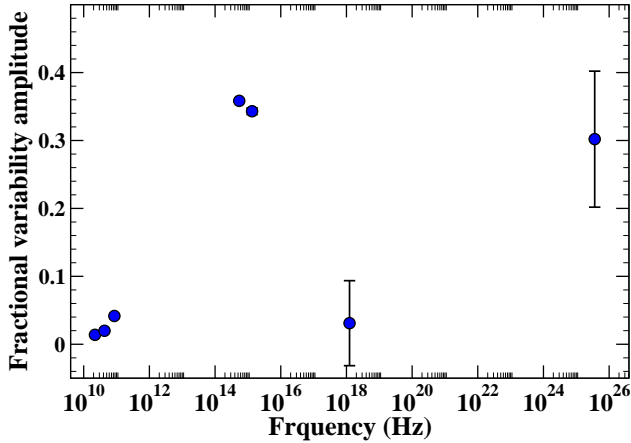


Figure 3.  $F_{var}$  amplitude spectrum of 3C 279 from radio to  $\gamma$ -rays.

– 300 GeV data of the source from December 28, 2013, to January 03, 2014. The LAT data were analyzed using the standard ScienceTools (software version v10.r0.p5) and instrument response functions P8R2\_SOURCE\_V6. Photons in the source event class were selected for the analysis. We analyzed a region of interest (ROI) of  $20^\circ$  radius centered at the position of 3C 279 using a maximum-likelihood algorithm (Mattox et al. 1996). In the unbinned likelihood analysis<sup>5</sup>, we included all sources of the 3FGL catalog (Acero et al. 2015) within  $20^\circ$  and the recommended Galactic diffuse background (*gll\_iem\_v06.fits*) and the isotropic background (*iso\_P8R2\_SOURCE\_V6\_v06.txt*) emission components (Acero et al. 2016). Model parameters for the sources within  $5^\circ$  of the center of the ROI were kept free. Beyond the  $5^\circ$  ROI, model parameters of the sources reported as being significantly variable (variability index  $\geq 72.44$ ) in the 3FGL catalog are kept free as well, while the parameters for the rest were fixed to their catalog values. To characterize the variability properties of the source, we generated the light curves using a time binning of one day. The daily binned light curves of the source at  $E > 100$  MeV were produced by modeling the spectra over each bin by a simple power law ( $N(E) = N_0 E^{-\Gamma}$ ,  $N_0$ : prefactor, and  $\Gamma$ : power law index). Variability at shorter timescales cannot be investigated as the source is not bright enough. The photon flux (a) and photon index (b) curves are shown in Fig. 1. We noticed a prominent flare in the photon flux light curve accompanied by no clear spectral variation; the average  $\gamma$ -ray photon index is  $2.4 \pm 0.2$ .

### 3 RESULTS

#### 3.1 Light curve analysis

Figure 1 shows the broadband light curves of the source observed between December 28, 2013, and January 03, 2014. At GeV energies, we observed an increase in the brightness of the source with a peak at  $JD^{*6} \sim 58.5$  (a); the horizontal green line marks the quiescent flux level<sup>7</sup>. The significance of variability is examined via a  $\chi^2$ -test (testing the hypothesis of a non-variable source). Variations in the  $\gamma$ -ray light curve are found to be marginally significant with

a significance level of  $2.4 \sigma$ ; however, no significant variation (significance level  $< 0.04 \sigma$ ) is noticed in the  $\gamma$ -ray photon index curve (b).

We noticed three peaks (labeled as X1 to X3) at X-ray energies. The first peak (X1) roughly coincides with a peak in the percentage polarization curve at radio bands. The peak X2 has an apparent coincidence with the peak in the optical/UV light curves. The last peak (X3) is observed about a day after the peak in the  $\gamma$ -ray light curve. Given the low significance of the entire X-ray light curve ( $\sim 1.4 \sigma$ ), we regard these flares as a possible hint of variability.

A prominent flare was observed in the source at optical (V band) and ultra-violet (M2 band) frequencies. The source brightened by a factor of two with a peak at  $JD^{*} \sim 58$  (e), which approximately coincides with the peak of the  $\gamma$ -ray flare. The estimated significance of variability is  $5.7 \sigma$  and  $4.9 \sigma$  respectively for the V and M2 band light curves. In Fig. 2 (b), we show the V–M2 color variations during the course of our observations. The V–M2 color characterizing the spectral slope in the optical-UV region has an average value of  $V - M2 = 0.05 \pm 0.04$  and shows no statistically significant ( $< 0.1 \sigma$ ) changes over the course of the observing campaign.

At radio frequencies, total flux and polarization of the source were observed at 22, 43, and 86 GHz. Radio flux density (f), linear polarization (g), and EVPA (h) curves of the source are displayed in Fig. 1. The source exhibits a marginal flux density variability at radio bands; however, variations are more pronounced in fractional polarization curves. The observed peak in the fractional polarization curve at 86 and 43 GHz coincides with the first peak, X1, in the X-ray light curve. Similar to total intensity, the EVPA values remain unchanged during our observations. The total intensity observations at 43 and 86 GHz radio bands are used to investigate the spectral index variations. We used a power law of the form  $P(\nu) \propto \nu^{-\alpha}$ , where  $\alpha$  is the spectral index, to get an estimate of radio spectral index. The radio spectral index variations are shown in Fig. 2 (a). During the four days of our observations, we noticed a clear steepening of the radio spectrum ( $\alpha$  changes from  $0.23 \pm 0.02$  to  $0.33 \pm 0.01$ ).

As we discussed above, the variability behavior is very complex and depends on the frequency observed. In the following sections, we investigate the nature of broadband flux variability and the possible correlation among the multi-frequency light curves of the source.

#### 3.2 Fractional variability

In order to quantify and compare the total variability at each observed band, we estimated the fractional variability amplitude,  $F_{var}$ , given by Vaughan et al. (2003):

$$F_{var} = \sqrt{\frac{S^2 - \overline{\sigma_{err}^2}}{\bar{x}^2}} \quad (1)$$

where  $S^2$  is the sample variance of the light curve,  $\bar{x}$  is the average flux and  $\overline{\sigma_{err}^2}$  is the mean of the squared measurement uncertainties. The uncertainties on  $F_{var}$  due to the measurement-error fluctuations have been estimated through Monte Carlo simulations by Vaughan et al. (2003, eq. B2).

The estimated  $F_{var}$  is plotted in Fig. 3. The  $F_{var}$  strongly depends on frequency. In the radio regime,  $F_{var}$  increases with frequency/energy and the trend continues until the optical/UV regime where it has a peak; an explanation for this is that the evolution

<sup>5</sup> [http://fermi.gsfc.nasa.gov/ssc/data/analysis/scitools/likelihood\\_tutorial.html](http://fermi.gsfc.nasa.gov/ssc/data/analysis/scitools/likelihood_tutorial.html)

<sup>6</sup>  $JD^{*} = JD - 2456600$

<sup>7</sup> The quiescent level is the photon flux value in the beginning of the outburst (November 2013).



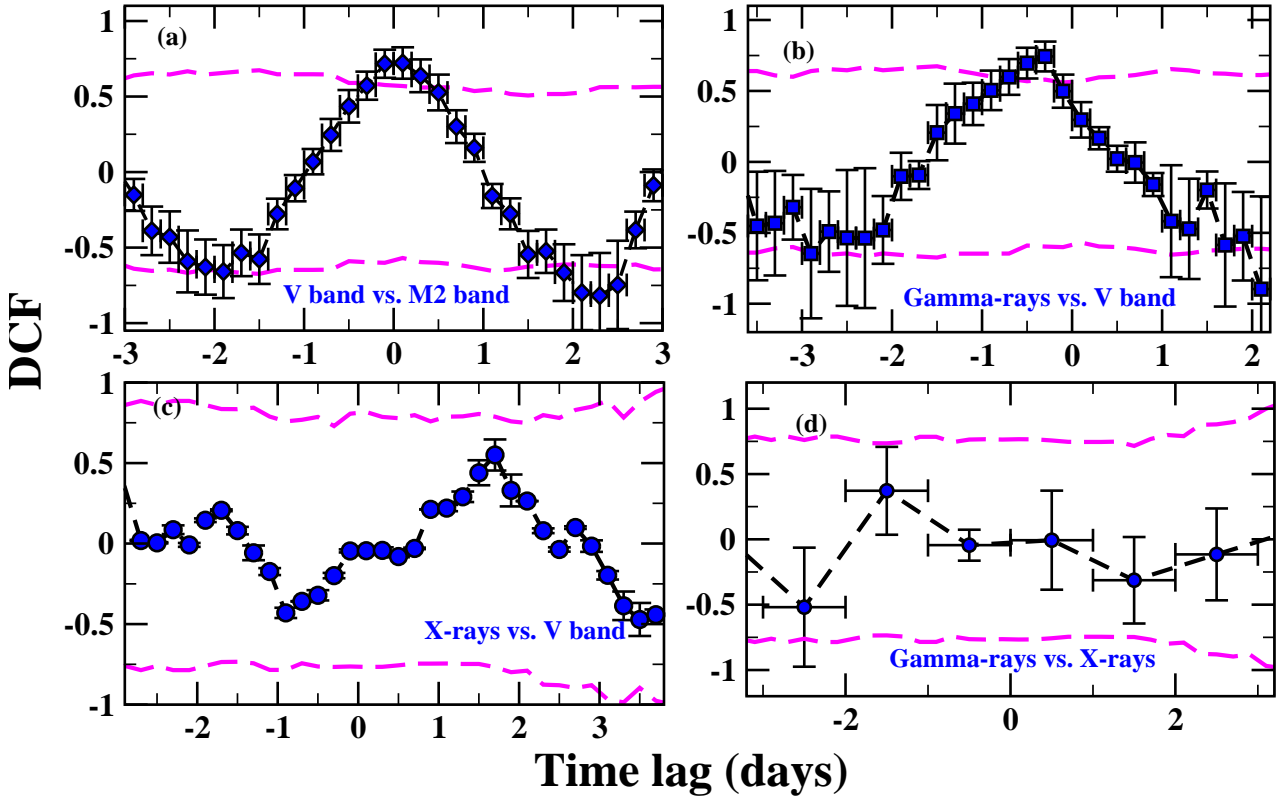


**Figure 4.** Cross-correlation analysis curves: (a) Optical V band vs. near-UV M2 band (bin size = 0.2 day), (b) Gamma-rays vs. Optical V band (bin size = 0.2 day), (c) X-rays vs. Optical V band (bin size = 0.2 day), and (d) Gamma-rays vs. X-rays (bin size = 1.0 day). The dashed lines denote the 95% confidence levels.

of synchrotron flares might propagate from higher to lower energies (Marscher & Gear 1985). The  $F_{var}$  peak is followed by a dip in the X-ray domain. The  $F_{var}$  vs. frequency plot (Fig. 3) resembles a double-hump structure, which has been noted previously for several blazars (Chidiac et al. 2016; Aleksić et al. 2015; Soldi et al. 2008). The double hump could be related to the two humps in the broadband SED (spectral energy distribution) of blazars, where the variability increases with frequency in each hump i.e. largest variations are seen for the highest energy electrons producing each hump.

### 3.3 Cross-correlation analysis

The discrete cross-correlation function (DCF, Edelson & Krolik 1988) method was used to quantify the correlation among the multi-frequency light curves of the source and to search for possible time lags. The details of this method are also discussed by Rani et al. (2009). As a conservative approach, we used half the duration of the observations, i.e.  $\pm 3.5$  days, as the correlation search time window. Depending on the sampling rate of the data used for the DCF analysis, a suitable bin size was chosen for each observing band (see Fig. 4 caption). The significance of the DCF analysis was tested using simulations as described in Appendix A of Rani et al. (2014). To estimate the confidence level for each DCF curve, we generated a series of 1000 light curves to obtain the upper and lower bands of the 95% confidence levels. The cross-correlation analysis results of the broadband light curves are shown in Fig. 4. The dashed lines in

Fig. 4 represent the 95%<sup>8</sup> confidence levels. In the following sections, we discuss in detail the cross-correlation analysis results.

#### 3.3.1 Optical vs. near-UV

A prominent flare is observed almost simultaneously in the optical (V passband) and near-UV (M2 passband) light curves, which is expected as the two passbands are very close in frequency. A significant correlation is observed between the flux variations at the two bands with a correlation coefficient  $0.65 \pm 0.10$  at a time lag of  $0.1 \pm 0.1$  days<sup>9</sup>, which is compatible with no time lag (Fig. 4 b). The DCF analysis therefore indicates that the flux variations in optical and near-UV bands are significantly correlated with no time lag longer than 0.2 day. Owing to its better time sampling, we will only use the V passband data for the DCF analysis with broadband light curves.

#### 3.3.2 Gamma-ray vs. optical

Visual inspection of the variability curves in Fig. 1 shows an apparent similarity between the  $\gamma$ -ray and optical flux variations. The DCF curve between the two shows a peak at  $-(0.3 \pm 0.1)$  days with a correlation coefficient  $0.74 \pm 0.10$  (Fig. 4 c) at a confidence level  $> 95\%$ . The analysis therefore suggests that the flux variations at

<sup>8</sup> Correlations having confidence levels above 95% are considered significant.

<sup>9</sup> The given uncertainty in the time lag value here and in the following sections is the half the bin size used for the DCF analysis.

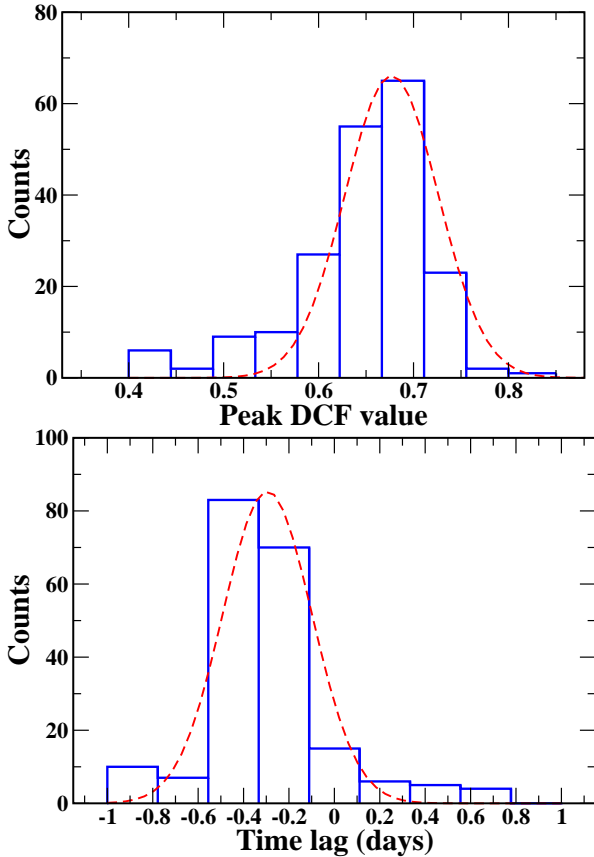


**Figure 5.** Histogram of peak DCF value (top) and time lag (bottom). The dashed-curve represents the fitted Gaussian function.

optical and  $\gamma$ -ray frequencies are significantly correlated with the former leading the latter by  $(0.3 \pm 0.1)$  days.

The estimated time lag ( $\sim 0.3$  day) between the optical and  $\gamma$ -ray flares is smaller than the time sampling of the  $\gamma$ -ray light curve (1 day). To determine how sensitive the estimated time lag is to the sampling rate of the given light curves, we used the interpolated cross correlation function (ICCF) method (Gaskell & Peterson 1987; Breedt et al. 2010). It is important to note that the simulations and interpolation take into account the observed profile of the light curve. If there are faster variations present but are not observed by any means (either due to low brightness or some other reasons), this method is not suitable for testing that. We implemented the ICCF method as follows. We interpolated each light curve and cross-correlated it with the other to test whether the sampling of the first one gives rise to spurious correlations. In the first case, we generated 100 interpolated  $\gamma$ -ray light curves having a time sampling from 0.02 to 2 days with a step-size of 0.02 day. The interpolated  $\gamma$ -ray light curves were then correlated with the observed optical light curve. We repeated the same procedure for the optical light curve and correlated the interpolated optical light curves with the observed  $\gamma$ -ray light curve. In total, we had 200 DCF curves that were used to estimate the peak DCF value and the corresponding time lag. Figure 5 shows the distribution<sup>10</sup> of the obtained DCF parameters (peak DCF values and time lags). We next investigated

<sup>10</sup> The number of cells for the histograms was calculated using the “Scott” algorithm available under the “hist” function in *R* (a language and environment for statistical computing), which computes a histogram

**Table 1.** Fitted parameters of flares

Flare observed at	$T_r$ (day)	$T_d$ (day)	$t_0$ (JD’)	$F_0$
Gamma-ray	$2.5 \pm 1.2$	$2.3 \pm 1.1$	$57.9 \pm 1.2$	$2.45 \pm 0.30$
Optical (V)	$0.4 \pm 0.1$	$1.8 \pm 0.4$	$57.1 \pm 0.3$	$1.94 \pm 0.31$
near-UV (M2)	$0.4 \pm 0.1$	$1.0 \pm 0.3$	$57.4 \pm 0.4$	$0.44 \pm 0.12$

Notes:  $F_0$  is in the units of mJy for optical and near-UV bands and is in  $10^{-6} \text{ ph cm}^{-2} \text{ s}^{-1}$  for  $\gamma$ -rays.

the distribution of the obtained DCF parameters to test how sensitive the estimated time lag ( $\sim 0.3$  day) is to the sampling of the observed light curves. The DCF parameter’s distribution can be well approximated via a Gaussian function, as is shown in Fig. 5. The estimated DCF value distribution has a peak at 0.65 with FWHM = 0.12. For the estimated time lags, the Gaussian function yields a peak at  $-0.24$  with FWHM = 0.14 days. It is therefore evident that the estimated time lag is not sensitive to the given sampling of the light curves.

In an alternative approach, we estimated the time corresponding to the peak of the optical/ $\gamma$ -ray flare by modeling their profiles with an exponential function. The flares at optical/ $\gamma$ -ray frequencies can be well approximated with an exponential rise and decay of the form (Rani et al. 2013b):

$$F(t) = 2 F_0 \left[ e^{(t-t_0)/T_r} + e^{(t-t_0)/T_d} \right]^{-1}, \quad (2)$$

where  $T_r$  and  $T_d$  are the rise and decay times, respectively, and  $F_0$  is the source flux at  $t_0$  representing the flare amplitude. The red curves in Fig. 6 represent the fitted flare components. In Table 1, we listed the fitted parameters.

Fig. 6 shows that the rise and decay timescales are very similar for the  $\gamma$ -ray flare, while the optical/near-UV flare has a relatively fast rise and slow decay. Within the error bars, the estimated time of the flare peak is similar at optical/near-UV and  $\gamma$ -ray energies, which suggests no time lag between the two. This is inconsistent with the DCF analysis results that suggests optical leading  $\gamma$ -rays by  $\sim 0.3$  day. The difference is most likely due to the faster rise of the optical/near-UV flare, which produces a time lag in the DCF analysis. Given the relatively mild variations and 1 day time sampling of the  $\gamma$ -ray light curve, we cannot prove that the optical leads the  $\gamma$ -ray emission. Since we found that the observed time lag seems not to be sensitive to the sampling of the observed light curve, however, we cannot ignore the possibility that the lag is real. Simultaneous observations at a higher cadence would be required to test the hypothesis. A correlated optical –  $\gamma$ -ray flare with optical leading  $\gamma$ -rays by  $\sim 22$  hrs was previously observed for PKS 1406–076 (Wagner et al. 1995). Such correlations seem not to be consistent with simple versions of high-energy emissions models, where one expects to see either high-energy flares followed by low-energy flares or simultaneous variations.

The simulation only tells us about the significance of correlation given the observational errors. It does not account for the possibility that the source has flares at random times in two bands and the times of flares are completely uncorrelated. It is therefore essential to compare the long-term behavior of the two light curves. We noticed a very similar flaring activity in the long-term optical/ $\gamma$ -ray light curves; the source displayed multiple flares superimposed

of the given data. Details are given at <https://stat.ethz.ch/R-manual/R-devel/library/graphics/html/hist.html>.

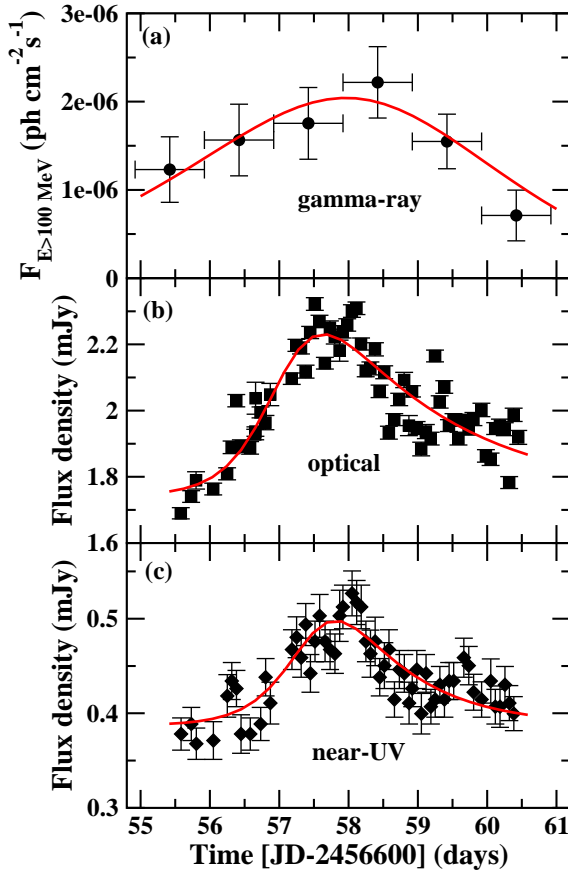


**Figure 6.** The modeled  $\gamma$ -ray (a), optical (b), and near-UV (c) flare in 3C 279 using an exponential function (see Section 3.3.2 for details). The black points are the observed data while the red curves represent the fit.

on top of a broad-outburst observed between November 2013 and August 2014. A comparison of the flaring activity suggests a significant correlation between the optical/ $\gamma$ -ray flaring activity, which supports the idea that the optical/ $\gamma$ -ray correlation reported here is not a random coincidence. A detailed analysis of the broadband flaring activity from November 2013 to August 2014 and its connection with the jet kinematics will be given in a separate paper (Rani et al. 2016, in preparation).

### 3.3.3 X-ray vs. optical and gamma-rays

We noticed a peak in the X-ray vs. optical V passband DCF analysis curve, with a correlation coefficient of  $0.53 \pm 0.10$  (see Fig. 4 d), which suggests a possible correlation between the two with the former leading the latter with a time lag of  $\sim 1.8$  days. The significance of the peak is  $\sim 90\%$ , however, below the 95% confidence level. The  $\gamma$ -ray vs. X-ray DCF analysis curve does not show any significant peak for the observations (Fig. 4 a). The DCF analysis therefore does not support a correlation between the two.

### 3.3.4 Radio vs. radio

Despite having a low fractional variability, variations at different radio bands seem to have similar behavior. In the total intensity curves, we noticed only marginal variations, and the same is the case for the EVPA curves. A micro-flare is observed in the fractional polarization curve both at 86 and 43 GHz radio bands. The

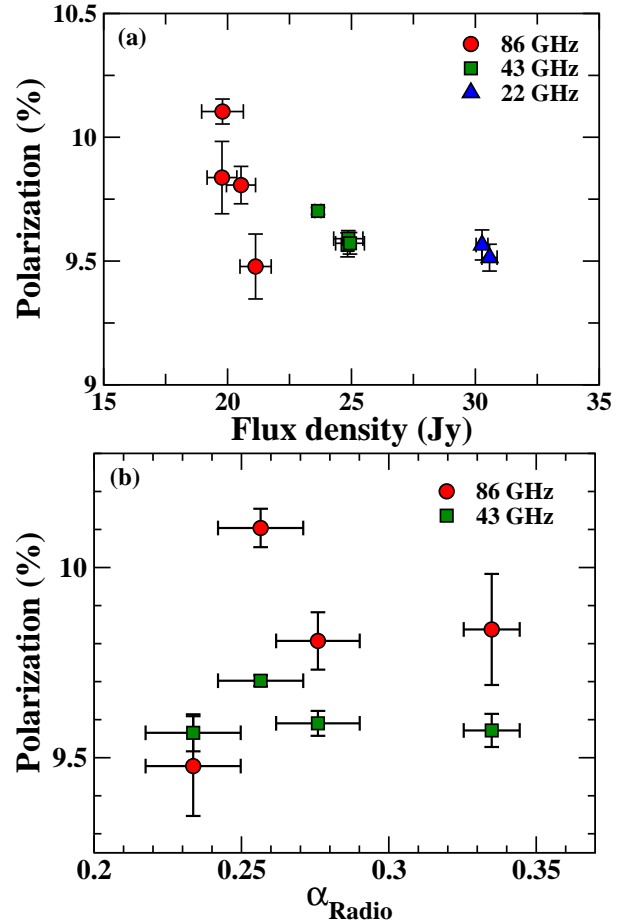


**Figure 7.** Fractional linear polarization plotted as a function of flux density (a) and spectral index (b) at different radio bands - red circles denote 86 GHz band, green squares denote 43 GHz band, and blue triangles denote 22 GHz band.

observed micro-flare has similar rise ( $\sim 1$  day) and decay ( $\sim 2$  days) timescales at the two radio bands, suggesting a possible correlation between the two. With only four measurements, the radio-radio correlation and also correlation with other bands cannot be tested via the formal DCF analysis method.

### 3.4 Flux density vs. linear polarization

Unlike the higher frequencies, the total intensity variations are milder at radio bands, but we observed a prominent micro-flare in the polarization curve at 86 and 43 GHz radio bands. Figure 7 shows the fractional linear polarization plotted as a function of flux density at different radio bands. The degree of polarization is higher at higher frequencies. In addition, there is an apparent anti-correlation between flux density and linear polarization for the source. A formal linear Pearson correlation analysis gives  $r_p = -0.64$  with a 95.4% confidence level, where  $r_p$  is the linear Pearson correlation coefficient. A systematic increase in the degree of linear polarization could be expected as Faraday depolarization effects decrease with increasing frequency.

Particularly at 86 GHz, a change in polarization degree (PD) occurred while the total intensity and EVPA were relatively constant. An increasing PD indicates a more ordered magnetic field or a steepening of the electron (and also synchrotron) spectrum.

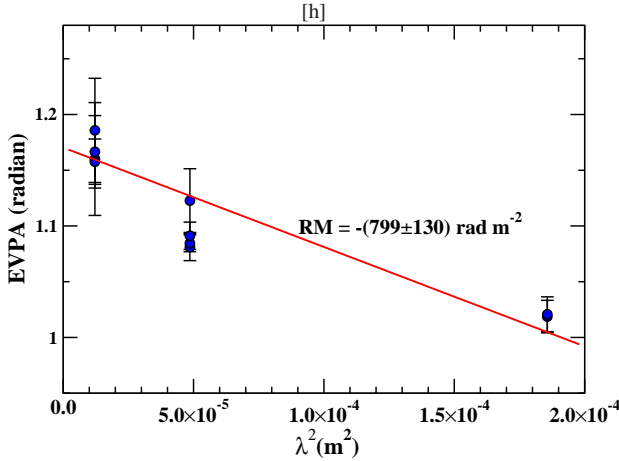


**Figure 8.** Dependence of EVPA (polarization position angle) on square of wavelength in 3C 279. The solid line represents the best fit.

The observations also show variations in the radio spectrum (see Fig. 2 a), as well as an indication of steepening of the radio spectrum with an increase in PD (see Fig. 7 b); however, with only four measurements, we cannot make a statistical claim. An increase in PD while the spectrum gets softer, although needs to be tested further using high cadence observations, provides an hint that the PD variations could be simply due to a spectral change<sup>11</sup> without any changes in the magnetic field.

### 3.5 Faraday Rotation Measure

Figure 1 (h) shows the EVPA variations measured at 22 (in blue), 43 (in green), and 86 GHz (in red) radio bands. The observed difference in the EVPA measurements at different radio bands can be used to obtain rotation measure (RM) estimates. In case of external rotation, the effect can be described by a linear dependence between the observed EVPA ( $\chi_{obs}$ ) and wavelength squared ( $\lambda^2$ ) by

$$\chi = \chi_0 + \frac{e^3 \lambda^2}{8\pi m_e^2 \epsilon_0 c} \int N(s) \vec{B}(s) \cdot ds \quad (3)$$

$$\chi = \chi_0 + RM \lambda^2 \quad (4)$$

where  $\chi_0$  is the intrinsic polarization angle,  $e$  is the electron charge,  $m_e$  is the electron mass, and the integral is taken over the line of sight from the source to the observer (Gabuzda et al. 2004). The EVPA values as a function of  $\lambda^2$  are plotted in Fig. 8, which could be well approximated by a linear fit. We obtained  $EVPA = -(799 \pm 130) \lambda^2 + 1.16 \pm 0.01$ . This implies a RM of  $-(799 \pm 130) \text{ rad m}^{-2}$ , which is consistent with the previous RM measurements in 3C279 (Zavala & Taylor 2001; Lee et al. 2015; Wardle et al. 1998; Jorstad et al. 2007). Much smaller RM values,  $RM \sim -(42 \text{ to } 74)$ , have also been reported for the source (Hovatta et al. 2012). In general, higher RM values are found at higher frequencies, which could be due to an external screen in the vicinity of the jet (Lee et al. 2015; Jorstad et al. 2007).

<sup>11</sup> The degree of linear polarization is equal  $\frac{(\alpha+1)}{\alpha+5/3}$  (Rybicki & Lightman 1986), where  $\alpha$  is the spectral index.

## 4 DISCUSSION AND CONCLUSIONS

Extremely bright GeV/TeV flares at minutes to hours timescales are a common characteristic of  $\gamma$ -ray-bright blazars. The rapid flares usually do not have a low-frequency counterpart (Rani et al. 2013a, 2015; Abdo et al. 2010a; Hayashida et al. 2012), making it difficult to interpret the radiation processes and acceleration mechanisms involved. We organized a multi-wavelength campaign to understand the physical processes responsible for the origin of extreme  $\gamma$ -ray flaring activity observed in 3C 279 in December 2013. The source was observed from radio (including polarization) to  $\gamma$ -rays.

A relatively mild  $\gamma$ -ray flare was observed in 3C 279 during our campaign period. Compared to the extremely bright and rapid flares ( $t_{var} \sim \text{few hours}$ ) seen at other times, this flare had relatively longer variability timescales ( $t_{rise}$  and  $t_{decay} \sim 2.5$  days). Nevertheless, the  $\gamma$ -ray flare was accompanied by a prominent flare at optical and near-UV passbands, and we found a significant correlation between the two. The optical/near-UV flare, however, had a relatively fast rise ( $\sim 0.4$  day) and slow decay ( $\sim 1.5$  days). The flux variations (both at optical and  $\gamma$ -ray frequencies) were accompanied by no significant spectral variations. Broadband spectral modeling of the flaring activity by Hayashida et al. (2015) for a period that has 3 days overlap with our observations suggests a substantial contribution of external-Compton radiation from the broad-line region. Their analysis also indicates that the location of the  $\gamma$ -ray emission region is comparable with the broad-line region radius. The observed optical- $\gamma$ -ray correlation suggests a co-spatiality of the two emission regions.

We observed a slight hint of variability (significance  $\sim 1.4 \sigma$ ) in the 0.3–10 keV X-ray light curve. The formal cross-correlation analysis suggests no correlation between the X-ray and  $\gamma$ -ray variations. There is a hint of possible correlation between the X-ray and the optical variations with the former leading the latter by  $\sim 1.8$  days; however, the confidence level of the correlation is below 95%. A micro-flare peaking in the fractional polarization curve at 43 and 86 GHz radio bands coincides with the first peak (X1) in the X-ray light curve. Observations at a better cadence would be needed to test this apparent correlation. Unlike the higher frequencies, the total intensity variations are not pronounced at radio bands. We noticed a micro-flare in polarization degree (PD), while the variations in EVPA curves are not statistically significant. An indication of spectral steepening at radio bands with an increase in PD suggests that the PD variations could be due to a spectral change without any change in the magnetic field (B-field).

The presence of contemporaneous optical/ $\gamma$ -ray flaring activity is not always the case for blazars. However, studies over the past few years indicate a similarity in the variability properties of the two bands (Cohen et al. 2014; Chatterjee et al. 2012), suggesting the same population of electrons being responsible for the synchrotron (optical) and inverse-Compton ( $\gamma$ -rays) radiation. For 3C 279, Hayashida et al. (2012) reported a good correlation between the optical and  $\gamma$ -ray flares in 2008–2012. However later in 2013–2014, this correlation seemed to be less obvious (Hayashida et al. 2015). A comparison of long-term optical/ $\gamma$ -ray flaring activity between November 2013 and August 2014 including our campaign period suggests a significant correlation between the two (Rani et al. 2016, in preparation). The observed optical-X-ray correlations in 3C 279 also present a complicated picture. A detailed analysis of the optical-X-ray correlations between 1996 and 2007 by Chatterjee et al. (2008) suggests that for some flares optical lead X-rays while for others it is vice-versa. Additionally, an orphan X-ray flare was observed in the source in 2008–2010



(Abdo et al. 2010a; Hayashida et al. 2012). Presence of multiple emission regions (Marscher 2014; Hayashida et al. 2015), different dependencies of magnetic field density and energy density of the external radiation field (Janiak et al. 2012), and/or particle acceleration in a stratified jet (Rani et al. 2013a, 2015) have all been suggested as plausible scenarios.

During our campaign period, a short-duration ( $\sim 5$  day) flare at optical/near-UV frequencies is found to be significantly correlated with a contemporaneous flare at  $\gamma$ -rays. The  $F_{var}$  at  $\gamma$ -ray does not exceed that at optical/near-UV bands, which is usually not what had been observed for 3C 279. The  $F_{var}$  at  $\gamma$ -rays is usually much higher than or at least comparable to that at optical frequencies (Hayashida et al. 2012, 2015; Rani et al. 2016, in preparation). The optical flare has a marginally significant correlation with the X-ray variations. Nearly simultaneous spectral analysis (Hayashida et al. 2015) suggests superposition of two spectral components, as a single-zone leptonic model failed to explain the X-ray spectrum. A coincidence of a micro-flare in the fraction of polarization at radio bands with the X-ray flare certainly emphasizes its jet base origin.

In a tentative scenario, a single population of electrons seems to be responsible for the optical/near-UV and  $\gamma$ -ray flares. X-rays could be produced via synchrotron self-Compton with seed photons coming from short-mm radio bands as is supported by the coincidence of the increase of radio polarization (at 43 and 86 GHz bands) with the X-ray flux. The X-ray flare leading the optical flare could be expected if the high-energy electrons take longer to accelerate compared to the lower-energy electrons (Böttcher 2007). As a consequence, the radio and X-ray flares lead the optical/ $\gamma$ -ray flares. An alternative explanation could be that the particles are accelerated in a different region. The presence of multiple sub-components in the emission could also be possible.

In leptonic models, the relative amplitude variations of synchrotron and IC flares could be simply determined by the B-field, the number of emitting electrons ( $N_e$ ), and the Doppler factor ( $\delta$ ) (Chatterjee et al. 2008). A spectral hardening at radio frequencies with an increase in polarization degree does not support the B-field variations. An increase in both  $N_e$  and  $\delta$  causes a larger enhancement in the IC-flux compared to the synchrotron flux (Chatterjee et al. 2008). As a result, one expects to see larger variability amplitude for the IC flare compared to the synchrotron flares; however, for our observations, the reverse is true. This could be because of different dependencies of B-field energy density and external radiation field energy density on the distance along the jet from the central engine (Janiak et al. 2012). It is important to note that we consider leptonic models for our interpretation; however, hadronic models are equally able to reproduce a similar kind of variability.

## 5 ACKNOWLEDGEMENTS

The *Fermi*/LAT Collaboration acknowledges the generous support of a number of agencies and institutes that have supported the *Fermi*/LAT Collaboration. These include the National Aeronautics and Space Administration and the Department of Energy in the United States, the Commissariat à l’Energie Atomique and the Centre National de la Recherche Scientifique / Institut National de Physique Nucléaire et de Physique des Particules in France, the Agenzia Spaziale Italiana and the Istituto Nazionale di Fisica Nucleare in Italy, the Ministry of Education, Culture, Sports, Science and Technology (MEXT), High Energy Acceler-

ator Research Organization (KEK) and Japan Aerospace Exploration Agency (JAXA) in Japan, and the K. A. Wallenberg Foundation, the Swedish Research Council and the Swedish National Space Board in Sweden. Additional support for science analysis during the operations phase is gratefully acknowledged from the Istituto Nazionale di Astrofisica in Italy and the Centre National d’Études Spatiales in France. This research was supported by an appointment to the NASA Postdoctoral Program at the Goddard Space Flight Center, administered by Universities Space Research Association through a contract with NASA. We would like to thank the referee for his/her constructive comments. BR acknowledges the help of M. Böttcher, Vassilis Karamanavis, Greg Madejski, Roopesh Ojha, Jeremy Perkins, and Dave Thompson for fruitful discussions and comments that improved the manuscript. BR is thankful to D. Emmanoulopoulos for the useful discussions on statistical analysis. The KVN is a facility operated by the Korea Astronomy and Space Science Institute. The KVN operations are supported by KREONET (Korea Research Environment Open NETWORK) which is managed and operated by KISTI (Korea Institute of Science and Technology Information). KVS is supported by the RFBR grant 14-02-31789. SSL and KS are supported by the National Research Foundation of Korea (NRF) grant funded by the Korea government(MSIP) (No. NRF-2016R1C1B2006697).

## REFERENCES

- Abdo A. A., et al., 2010a, *Nature*, **463**, 919
- Abdo A. A., et al., 2010b, *ApJ*, **716**, 30
- Acero F., et al., 2015, *ApJS*, **218**, 23
- Acero F., et al., 2016, *ApJS*, **223**, 26
- Albert J., et al., 2008, *Science*, **320**, 1752
- Aleksić J., et al., 2015, *A&A*, **576**, A126
- Atwood W. B., et al., 2009, *ApJ*, **697**, 1071
- Bertin E., Arnouts S., 1996, *A&AS*, **117**, 393
- Böttcher M., 2007, *Ap&SS*, **309**, 95
- Böttcher M., et al., 2007, *ApJ*, **670**, 968
- Breedt E., et al., 2010, *MNRAS*, **403**, 605
- Burbidge E. M., Rosenberg F. D., 1965, *ApJ*, **142**, 1673
- Burrows D. N., et al., 2005, *Space Sci. Rev.*, **120**, 165
- Chatterjee R., et al., 2008, *ApJ*, **689**, 79
- Chatterjee R., et al., 2012, *ApJ*, **749**, 191
- Chidiac C., et al., 2016, *A&A*, **590**, A61
- Cohen D. P., Romani R. W., Filippenko A. V., Cenko S. B., Lott B., Zheng W., Li W., 2014, *ApJ*, **797**, 137
- Collmar W., et al., 2010, *A&A*, **522**, A66
- Cutini S., 2015, The Astronomer’s Telegram, **7633**, 1
- Edelson R. A., Krolik J. H., 1988, *ApJ*, **333**, 646
- Gabuzda D. C., Murray É., Cronin P., 2004, *MNRAS*, **351**, L89
- Gaskell C. M., Peterson B. M., 1987, *ApJS*, **65**, 1
- Gu M., Cao X., Jiang D. R., 2001, *MNRAS*, **327**, 1111
- Hartman R. C., et al., 1996, *ApJ*, **461**, 698
- Hayashida M., et al., 2012, *ApJ*, **754**, 114
- Hayashida M., et al., 2015, *ApJ*, **807**, 79
- Homan D. C., Lister M. L., Aller H. D., Aller M. F., Wardle J. F. C., 2009, *ApJ*, **696**, 328
- Hovatta T., Lister M. L., Aller M. F., Aller H. D., Homan D. C., Kovalev Y. Y., Pushkarev A. B., Savolainen T., 2012, *AJ*, **144**, 105
- Janiak M., Sikora M., Nalewajko K., Moderski R., Madejski G. M., 2012, *ApJ*, **760**, 129
- Jorstad S. G., Marscher A. P., Lister M. L., Stirling A. M., Cawthorne T. V., Gómez J.-L., Gear W. K., 2004, *AJ*, **127**, 3115
- Jorstad S. G., et al., 2007, *AJ*, **134**, 799
- Kalberla P. M. W., Burton W. B., Hartmann D., Arnal E. M., Bajaja E., Morras R., Pöppel W. G. L., 2005, *A&A*, **440**, 775

- Kang S., Lee S.-S., Byun D.-Y., 2015, *Journal of Korean Astronomical Society*, **48**, 257
- Larionov V. M., et al., 2008, *A&A*, **492**, 389
- Lee S.-S., et al., 2011, *PASP*, **123**, 1398
- Lee S.-S., et al., 2014, *AJ*, **147**, 77
- Lee S.-S., Kang S., Byun D.-Y., Chapman N., Novak G., Trippe S., Algaba J. C., Kino M., 2015, *ApJ*, **808**, L26
- Lister M. L., et al., 2013, *AJ*, **146**, 120
- Maraschi L., et al., 1994, *ApJ*, **435**, L91
- Marscher A. P., 2014, *ApJ*, **780**, 87
- Marscher A. P., Gear W. K., 1985, *ApJ*, **298**, 114
- Mattox J. R., et al., 1996, *ApJ*, **461**, 396
- Mead A. R. G., Ballard K. R., Brand P. W. J. L., Hough J. H., Brindle C., Bailey J. A., 1990, *A&AS*, **83**, 183
- Paliya V. S., 2015, *ApJ*, **808**, L48
- Poole T. S., et al., 2008, *MNRAS*, **383**, 627
- Rani B., Wiita P. J., Gupta A. C., 2009, *ApJ*, **696**, 2170
- Rani B., et al., 2013a, *A&A*, **552**, A11
- Rani B., Lott B., Krichbaum T. P., Fuhrmann L., Zensus J. A., 2013b, *A&A*, **557**, A71
- Rani B., Krichbaum T. P., Marscher A. P., Jorstad S. G., Hodgson J. A., Fuhrmann L., Zensus J. A., 2014, *A&A*, **571**, L2
- Rani B., Krichbaum T. P., Marscher A. P., Hodgson J. A., Fuhrmann L., Angelakis E., Britzen S., Zensus J. A., 2015, *A&A*, **578**, A123
- Roming P. W. A., et al., 2005, *Space Sci. Rev.*, **120**, 95
- Rybicki G. B., Lightman A. P., 1986, *Radiative Processes in Astrophysics*
- Soldi S., et al., 2008, *A&A*, **486**, 411
- Taylor G. B., 2000, *ApJ*, **533**, 95
- Vaughan S., Edelson R., Warwick R. S., Uttley P., 2003, *MNRAS*, **345**, 1271
- Wagner S. J., Mannheim K., 2001, in Laing R. A., Blundell K. M., eds, *Astronomical Society of the Pacific Conference Series Vol. 250, Particles and Fields in Radio Galaxies Conference*. p. 142
- Wagner S. J., et al., 1995, *ApJ*, **454**, L97
- Wardle J. F. C., Homan D. C., Ojha R., Roberts D. H., 1998, *Nature*, **395**, 457
- Wehrle A. E., et al., 1998, *ApJ*, **497**, 178
- Woo J.-H., Urry C. M., 2002, *ApJ*, **579**, 530
- Zavala R. T., Taylor G. B., 2001, *ApJ*, **550**, L147